



# Assessment of High Porosity Lattice Structures for Lightweight Applications

Rita Ambu<sup>1</sup>(✉)  and Michele Cali<sup>2</sup> 

<sup>1</sup> Department of Mechanical, Chemical and Materials Engineering, University of Cagliari,  
Via Marengo 2, 09123 Cagliari, Italy

rita.ambu@unica.it

<sup>2</sup> Department of Electric, Electronics and Computer Engineering, University of Catania,  
Viale A. Doria 6, 95125 Catania, Italy

michele.cali@unict.it

**Abstract.** Additive manufacturing (AM) methods have a growing application in different fields such as aeronautical, automotive, biomedical, and there is a huge interest towards the extension of their use. In this paper, lattice structures for AM are analysed with regards to stiffness and printability in order to verify the suitability for applications where the main requirement of efficiency in terms of stiffness has to be balanced with other needs such as weight saving, ease of manufacturing and recycling of the material. At this aim, lattice structures with high porosity unit cells and large cell size made of a recyclable material were considered with a geometrical configuration allowing 3D printing without any supports. The lattice structures considered were based on body-centred cubic (BCC) and face centred cubic (FCC) unit cell combined with cubic cell. Finally, a multi-morphology lattice structure obtained by mixing different unit cells is also proposed. The lattice structures were modelled and structurally analysed by means of finite element method (FEM), manufactured with a Fusion deposition modelling (FDM) printer and evaluated in relation to printability and dimensional accuracy. The results show that the proposed structure with mixed cells is potentially advantageous in terms of weight saving in relation to the mechanical properties.

**Keywords:** Lattice structure · Additive manufacturing · Supportless 3D printing · Geometrical configuration · High porosity

## 1 Introduction

The relevance of Additive manufacturing (AM) techniques has grown over the years since these methods have shown to be potentially advantageous in different fields of application. These include aerospace industry, automotive and biomedical field where AM is used in surgery for preoperative planning, implants or medical devices with many benefits since it allows to design devices customized according to the patients' needs [1]. Generally, a main goal in the design of additive manufacturing is to reduce the overall weight of a component satisfying at the same time structural requirements. This process is promoted by the capability of AM to produce complex geometries providing designers

in this way with a greater freedom. Besides appropriate geometries, lightening of a component can be obtained by means of porous or lattice structures. These structures can be obtained with different methods and can take up part of the geometry of the component or can be the structure itself.

In particular, topology optimization and generative design usually generate geometries of the components with non-functional areas lightened by a porous, stochastic distribution of the material according to loads and constraints acting on the part [2]. On the other hand, non-stochastic, or regular, structures can be modelled with different procedures. In particular, these structures can be built in Computer Aided Design (CAD) environment by replicating a unit cell along the three Cartesian directions, to obtain lattice-based geometries. Regular architectures can also be obtained by means of the Implicit Function Modelling (IFM) which is used, in particular, to obtain structures based on triply periodic minimal surfaces (TPMS) such as Gyroids, Diamond, Schwarz P-cell and others reported in literature [3]. The application of IFM requires a more computational effort with respect to the CAD method; however, complex geometrical configurations with local variable relative density and cell size can be generated, while it is more difficult to obtain geometries with local variable properties with CAD method.

Lattice structures have been considered in different areas for their lightness, structural properties and, in particular, for their energy absorption capability which is of interest in aerospace, automotive and marine structural components. Different geometries have been proposed including prisms, octet-truss, and similar [4–6].

In this paper lattice structures were considered and evaluated in terms of stiffness and printability [7, 8] for general purpose applications where the main requirement of efficiency in terms of stiffness and energy absorption is asked to be balanced with other needs such as lightness, material saving, ease of manufacturing and recycling. An example of a potential application is relative to packaging for breakable or sensitive components where requirements include lightness and recycling features for an optimal performance. AM lattice structures potentially offer the opportunity to accomplish these requirements as well as the possibility of creating personalized packaging which can be of interest for the final consumer.

Two different unit cells were considered. The first unit cell is obtained as a combination of a simple cubic (SC) unit cell and a body-centred cubic unit cell (BCC), while the other is a combination of the first unit cell and the face centred cubic (FCC) unit cell. Most of the research reported in literature analyses structures made with the basic unit cells BCC and FCC manufactured with metallic materials [9, 10], while others studies analyse the effect, in terms of structural performance, of the addition of struts with different orientations to these basic unit cells [11]. The application of structures made with unit cells similar to those considered in this study is mainly relative to the design of bone scaffolds made with biocompatible metal alloys [12, 13] where architectures with small cell size and tailored properties are required for an optimal performance.

High porosity structures with a large cell size made of a thermoplastic material were analysed, in order to verify the feasibility of these structures regarding stiffness and efficiency in manufacturing, considered that these are characterized by a reduced strut size with respect to cell size. Generally, the stiffness of a lattice structure depends on the geometrical arrangement and size of the struts [14, 15] and increases with larger

strut size. It is also related to manufacturing, so that appropriate printing parameters have to be chosen in relation to the geometry and size of the lattice structure [16, 17]. As for manufacturing, the geometries considered in this study do not require supports for printing, which is advantageous for material saving. The models were structurally assessed with finite element analysis (FEA) by calculating the effective compressive and shear stiffness. Based on the numerical results obtained, a multi-morphology structure was finally proposed, modelled with both types of unit cells under study. This kind of structure is characterized by a variable volume fraction which can be also useful. The proposed structure was also evaluated by means of FE analysis, showing a good balance between stiffness and lightness. The lattice structures analyzed were 3D printed with Fusion deposition modelling (FDM) by using Polyethylene Terephthalate Glycol (PET-G), a thermoplastic polyester material with recycling capabilities. The 3D printed models were evaluated, in particular, in relation to the dimensional accuracy with respect to the CAD models. The results show that the lattice structures considered maintain adequate characteristics as for stiffness and manufacturing and can be useful when a main concern is lightness and material saving.

## 2 Modelling and Assessment of Lattice Structures

### 2.1 Modelling of Lattice Structures

The lattice unit cells were obtained by using a commercial parametric CAD modeller and the geometrical configurations are reported in Fig. 1. A simple cubic (SC) unit cell was combined with the unit cell body-centred cubic (BCC) to obtain the unit cell reported in Fig. 1a, that can be referred as SC-BCC. Then, the combination between the unit cell SC-BCC and the unit cell face-centred cubic (FCC) was considered to obtain the resulting unit cell reported in Fig. 1b, that can be referred as SC-BCC-FCC.

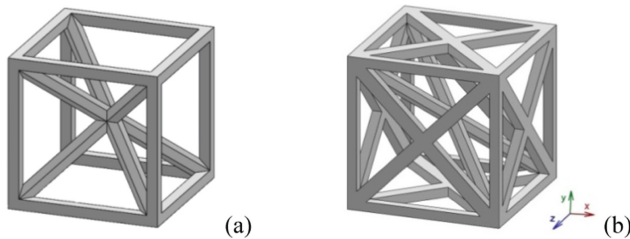


**Fig. 1.** Lattice unit cells: (a) SC-BCC; (b) SC-BCC-FCC.

A lattice structure is characterized by a value of the volume fraction given by  $V/V_0$ , namely, this parameter is defined as the ratio of the volume of the struts ( $V$ ) to the equivalent volume occupied by the porous structure ( $V_0$ ). The parameter can also be expressed in terms of porosity ( $P$ ) by considering the relationship:  $P = (V_0 - V)/V_0$ , which is generally expressed in terms of percentage.

The analysis performed was aimed to structurally evaluate high porosity structures. Therefore, a volume fraction of 0.10 equivalent to a porosity of 90% was considered.

In this way, it was possible to evaluate the effect of the geometry on the structural performance regardless of this parameter, which contributes to determine the stiffness of the structure. Lattice unit cells were designed assuming a cell size of 20 mm. A three-dimensional periodic array of the unit cell was then carried out along three mutually perpendicular directions to obtain the final architectures, each made of  $4 \times 4 \times 4$  cells. The number of cells of the models chosen for simulation allows to minimize the error in elastic modulus evaluation as shown in [18] where the variation of the stiffness of lattice models with different geometries by varying the number of cells was analysed. An evaluation of the mass of the two structures showed that SC-BCC unit cell allowed to produce a structure with a weight of about 42% lower with respect to that made of SC-BCC-FCC unit cells.

## 2.2 Numerical Assessment

The lattice structures were structurally analyzed by means of Finite Elements (FE) method. Each model was imported in a FE commercial software and meshed by using four nodes tetrahedral elements. Convergence testing was carried out in order to minimize the influence of mesh density on the results. The material chosen was Polyethylene Terephthalate Glycol (PETG), a thermoplastic resin whose mechanical properties are:  $E = 2100 \text{ MPa}$ ,  $\nu = 0.3$ .

First of all, each model was subjected to compression load. Uniaxial compression tests were performed by applying a uniform displacement, within the material elastic limit, to the top surface of the structure corresponding to 0.1% of compressive strain while the lower surface was fully constrained.

Figure 2 reports an iso-colour representation of Von Mises stress distribution, expressed in MPa, relative to the analyzed structures.

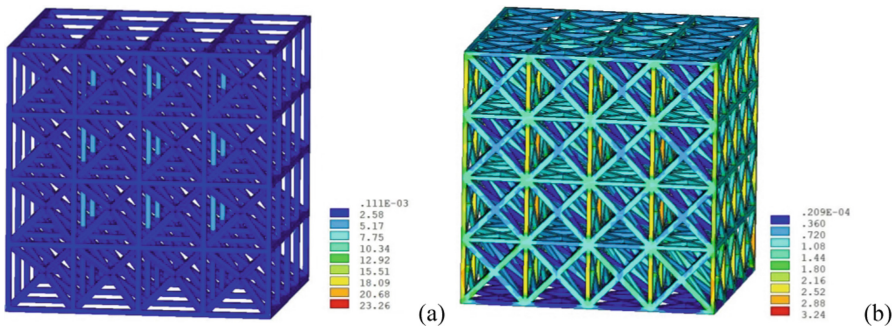


**Fig. 2.** Iso-colour representation of Von Mises stresses of lattice structures for compression loading: (a) SC-BCC; (b) SC-BCC-FCC

From the figure it can be observed that the lattice structure SC-BCC-FCC has a more homogeneous stress distribution with respect to the SC-BCC geometry. In fact, the SC-BCC structure is mainly affected by local stress concentration at the unit cell node of BCC lattice component which is induced by small radii corners of nodes. Researches on

the failure mechanism of the BCC lattice structure showed that the stress concentration is the main cause [19] and a reduction of this effect can be obtained with appropriate design [20]. This effect is attenuated instead in the other structure for the presence of the FCC geometry.

For each model, the effective elastic modulus ( $E_{\text{eff}}$ ) was evaluated based on Hooke's law. The reaction force was calculated by the FE solver while the homogenized stress was obtained by dividing the total reaction force by the total area of the loading plane. Since the applied strain is known,  $E_{\text{eff}}$  can be calculated.

The models were then subjected to shear load in order to evaluate the effective shear modulus ( $G_{\text{eff}}$ ). With reference to the coordinate system reported in Fig. 1 with the origin considered coincident with the barycentre of each model, the shear modulus was evaluated by the application of a uniform displacement to the nodes on the outermost lateral face (+x) in the y direction, while the opposite face (-x) was fully constrained. The nodes on the top face (+y) of each model and those on the bottom face were also constrained in the x direction. The parameter of interest, analogously to the procedure previously described for  $E_{\text{eff}}$ , was evaluated starting from the reaction force calculated by the FE solver. The equivalent applied strain was 0.1%.

The graph reported in Fig. 3 depicts the effective compressive modulus and the effective shear modulus for the lattice structures analyzed.

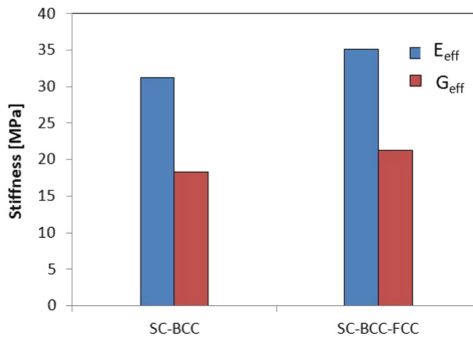


**Fig. 3.** Stiffness of lattice structures.

The lattice geometry SC-BCC-FCC shows higher values, both for  $E_{\text{eff}}$  and  $G_{\text{eff}}$ , compared to the other structure considered. Both structures show acceptable values of stiffness; however, SC-BCC-FCC structure can be considered as more efficient in terms of mechanical performance, also taking into account that, as previously observed, this geometrical configuration has a more homogeneous stress distribution with respect to the other considered.

However, as observed at the end of the previous paragraph, SC-BCC lattice structures, for the same volume fraction, are lighter than structures made of SC-BCC-FCC unit cells. Therefore, with the aim to reduce the overall weight, keeping at the same time adequate mechanical properties, a different structure was considered. This structure was obtained by combining both types of cells previously analysed so as to produce a multi-morphology lattice structure. In [21] it was shown that multi-morphology architectures

are also advantageous since they can lead to improved energy absorption. In particular, the structure was obtained by introducing SC-BCC unit cells on the inside, while the unit cells located externally were modelled as SC-BCC-FCC cells. Figure 4 reports the lattice structure obtained by using the proposed approach.

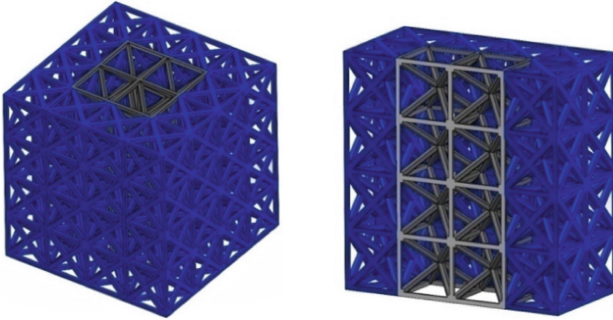


Fig. 4. Lattice structure made of mixed lattice cells.

In order to obtain a consistent solid model, an analogous size of the vertical struts for the two types of cells is required, to allow their superposition. This led to a slight increase, about 4%, of the volume fraction of the exterior component of the model. This structure, which was obtained by introducing  $2 \times 2 \times 4$  (25%) lighter SC-BCC unit cells, allowed to reach a weight reduction of about 7% with respect to a structure with uniform unit cell type.

The hybrid model was structurally analyzed by means of FE analysis and the stiffness for compressive loading ( $E_{eff}$ ) and shear loading ( $G_{eff}$ ) was evaluated. Figure 5 shows the results obtained in comparison with the corresponding, in terms of volume fraction, uniform SC-BCC-FCC lattice structure.

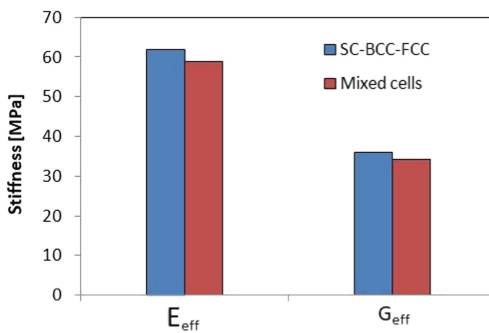


Fig. 5. Comparison of stiffness between uniform and mixed cells lattice structure.

The results obtained show a decrease of the stiffness in the hybrid structure, as expected, but with a limited difference between the values, assessing that this kind of approach is of interest for applications where weight reduction is a main requirement.

### 3 Manufacturing and Dimensional Assessment of Lattice Structures

#### 3.1 Manufacturing with FDM Printer

The designed geometries were printed from a stereolithography (STL) file with the commercial Delta-type Anycubic Chiron printer using the PET-G material and the mold parameters shown in Table 1.

The FDM technique adopted allowed an accurate printing of the lattice structures without support, avoiding the delicate phase of supports removal, also with saving of material and time.

**Table 1.** Main printing parameters adopted.

Parameter	Working value	Variation range	Parameter	Working value	Variation range
Layer thickness [mm]	0.2	0.1–0.5	Print velocity [mm/s]	20	5–210
Initial thickness [mm]	0.3	0.1–0.6	Filling velocity [mm/s]	50	5–210
Perimeter threads	2	1- $\infty$	Outer wall print velocity [mm/s]	20	5–210
Horizontal expansion %	0	0–100	Lower surface print vel. [mm/s]	30	5–210
N° upper layers	3	1– $\infty$	Movement velocity [mm/s]	100	5–210
N° lower layers	3	1– $\infty$	Lower layers print vel. [mm/s]	25	5–210
Fill density	20	10–30	Print acceleration [mm/s <sup>2</sup> ]	1000	0–1000
Fill configuration	Zig Zag	–	Feedback distance [mm]	6	0–300
Print temperature [°C]	230	180–240	Feedback velocity [mm/s]	40	30–60
Print bed temperature [°C]	70	20–100	Fan speed %	100	0–100
Flow %	100	0–100	Print bed adhesion type	Brim	–
Initial layer flow %	105	0–100	Brim line number	3	1– $\infty$

Figure 6 shows the printed lattice structures SC-BCC, SC- BCC-FCC, and the structure with mixed cells previously discussed.

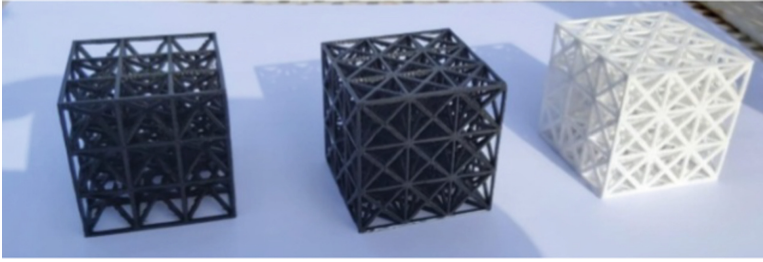


**Fig. 6.** Lattice structures obtained with 3D Anycubic Chiron printer: SC-BCC (at left), SC-BCC-FCC (at center), Mixed-cells lattice (at right).

The lattice structures were manufactured by enabling the control of the acceleration and variability of the feedback of the head (nozzle). Z Hop was also been enabled during print retraction and cooling. These settings, together with the arrangement of the printing parameters used, make possible to limit only to the “Layer thickness” and the “Feedback velocity”, the variations of the printing parameters necessary during prints without support with PET-G material. Among the printing parameters adopted, these, in fact, were the most critical ones for the accuracy of the printed models as the environmental conditions of temperature and humidity varied.

Using the printing parameters shown in Table 1, it was possible to optimize the values of the “Layer thickness” and the “Feedback velocity” as temperature and humidity changed (Fig. 7). The values shown in Fig. 7 allow to print the structures with considerable accuracy (see 3.2 subsection), without suffering appreciable flexural effects due to overhang.

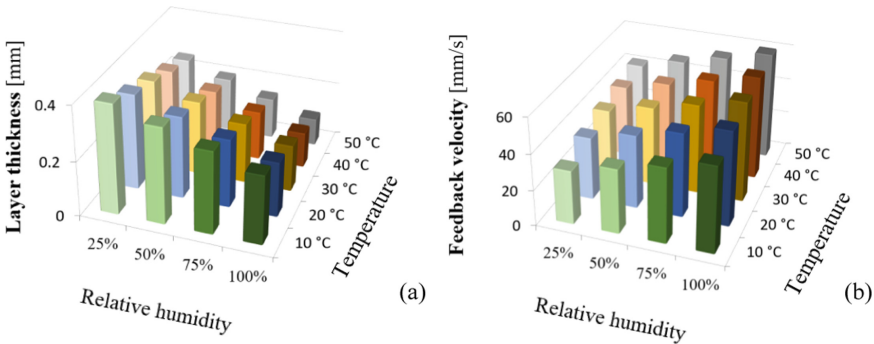


**Fig.7.** Printing parameters: (a) Layer thickness; (b) Feedback velocity.

The dimensions of the unit cells ( $20 \times 20 \times 20$  mm) and the geometric layout adopted in the printed lattice structures ensure that the sections of the structure always have inclinations less than or equal to  $45^\circ$ . In particular, the inclined struts inside the cube are inclined respectively at angles of  $35.26^\circ$  (Fig. 8a) and  $45^\circ$  (Fig. 8b).



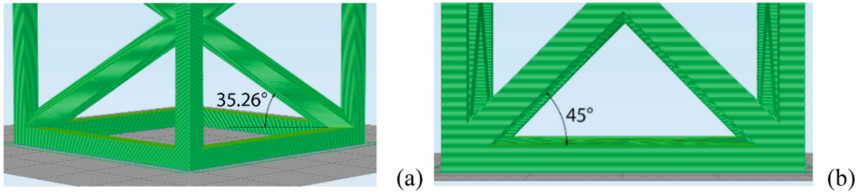


**Fig.8.** Inclined struts inside the unit cell: (a) 35.26° inclined struts; (b) 45° inclined struts.

### 3.2 Dimensional Assessment of 3D Printed Cellular Structures

Three special Azure Kinect DK sensors, equipped with advanced artificial intelligence system, were used to detect and quantify with high accuracy printing errors on the above-mentioned lattice structures (Fig. 9). Each Kinect sensor contains a depth sensor, camera and orientation sensor and, thus, is a compact “all-in-one” device usable with multiple modes by compiling the appropriate subroutines in Matlab environment. The most complete and accurate acquisitions (accuracy of 0.01 mm) were obtained by arranging 3 DK sensors at 120° around each printed structure (Fig. 9b).

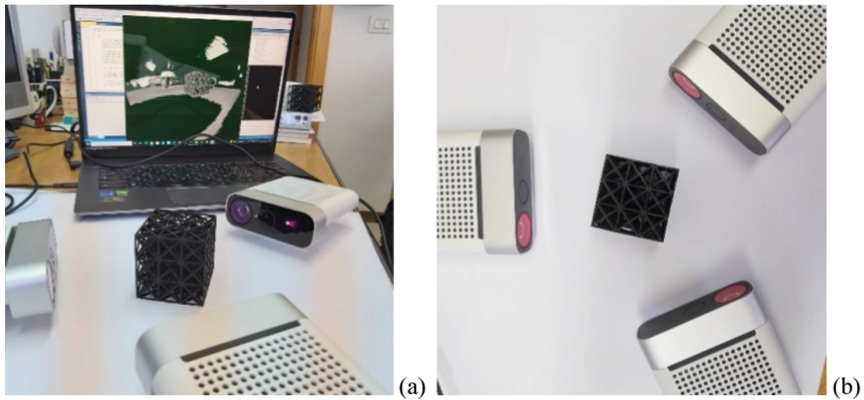


**Fig. 9.** (a) Azure Kinetic DK sensors acquisition system setup; (b) acquisition layout.

The acquisition with the three special Azure Kinect DK sensors has made possible to evaluate the printing errors for all the lattice structures manufactured. Figure 10 shows the comparison, in terms of dimensional deviation, between the proposed lattice with mixed cells structure printed with Anycubic Chiron printer using the PET-G and the designed STL model relative to the mixed-cells structure.

In detail, it was found that the maximum error occurs on the struts of the upper zone, which were printed last. In particular, the maximum positive errors (dimensions greater than the design ones) of magnitude equal to 0.22 mm occurred on the horizontal struts of the ends of the cubic structure, while the negative ones (dimensions smaller than the design ones) of magnitude equal to  $-0.12$  mm occurred on the struts inclined by 45° in the central area of the cube (Fig. 10).

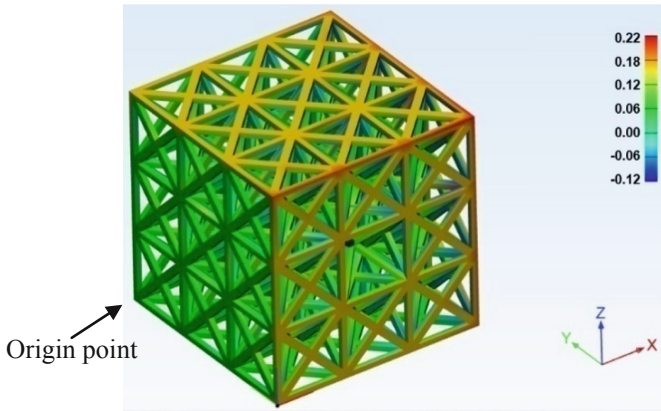


**Fig. 10.** Dimensional deviation between the printed structure and the STL model.

## 4 Conclusions

High porosity lattice structures for AM were analyzed in terms of stiffness and printability. Appropriate geometrical configurations of the unit cells with low strut size in relation to cell size have proven a satisfactory performance in terms of stiffness and accuracy in printing. The hybrid structure proposed can further reduce the overall weight with a limited decrease of stiffness. With the approach suggested in this study, potentially, the different type of unit cells should be easily arranged as required and the percentage of lighter unit cells can be varied, according to the final geometry of the part, considered that libraries of the basic unit cells could also be made available. As for manufacturing, support-less 3D printing has shown to be advantageous in terms of material as well preserving the dimensional accuracy of the produced parts.

## References

1. Praveena, B.A., Lokesh, N., Buradi, A., Santhosh, N., Praveena, B.L., Vignesh, R.: A comprehensive review of emerging additive manufacturing (3D printing technology): methods, materials, applications, challenges, trends and future potential. *Materials Today: Proceedings* **52**, 99–110 (2022)
2. Vlah, D., Žavbi, R., Vukašinović, N.: Evaluation of topology optimization and generative design tools as support for conceptual design. In: *International Design Conference-DESIGN 2020*, pp. 451–460. Cambridge University Press, England (2020)
3. Gabbriellini, R., Turner, I.G., Bowen, C.R.: Development of modelling methods for materials to be used as bone substitutes. *Key Engineering Materials* 361–363, Daculsi, G., Layrolle, P., Eds.: Scientific.net: Zurich, Switzerland, pp. 903–906 (2008)
4. Niu, J., Choo, H.L., Sun, W.: Finite element analysis and experimental study of plastic lattice structure manufactured by selective laser sintering. *Proceedings of the Institution of Mechanical Engineers, part L. Journal of materials: Design and Applications* **231**(1–2), 171–178 (2017)
5. Dong, L., Deshpande, V., Wadley, H.: Mechanical response of Ti–6Al–4V octet-truss lattice structures. *Int. J. Solids Struct.* **60–61**, 107–124 (2015)

6. Horn, T.J., Harrysson, O.L.A., Marcellin-Little, D.J., West, H.A., Lescelles, B.D.X., Aman, R.: Flexural properties of Ti6AlV4 rhombic dodecahedron open cellular structures fabricated with electron beam melting. *Addit. Manuf.* **1–4**, 2–11 (2014)
7. Tao, W., Leu, M.C.: Design of lattice structure for additive manufacturing. In: *International Symposium on Flexible Automation (ISFA) IEEE*, pp. 325–332 (2016)
8. Plocher, J., Panesar, A.: Review on design and structural optimization in additive manufacturing: towards next-generation lightweight structures. *Mater. Des.* **183**, 108164 (2019)
9. Ren, X.L., Xiao, L., Hao, Z.: Multi-property cellular material design approach based on the mechanical behaviour analysis of the reinforced lattice structure. *Mater. Des.* **174**, 107785 (2019)
10. Lee, K.-W., Lee, S.-H., Noh, K.-H., Park, J.-Y., Cho, Y.-J., Kim, S.-H.: Theoretical and numerical analysis of the mechanical responses of BCC and FCC lattice structures. *J. Mech. Sci. Technol.* **33**(5), 2259–2266 (2019)
11. Fadeel, A., Mian, A., Al Rifaie, M., Srinivasan, R.: Effect of vertical strut arrangements on compression characteristics of 3D printed polymer lattice structures: experimental and computational study. *J. Mater. Eng. Perform.* **28**(2), 709–716 (2018)
12. Wang, L., Kang, J., Sun, C., Li, D., Cao, Y., Jin, Z.: Mapping porous microstructures to yield desired mechanical properties for application in 3D printed bone scaffolds and orthopaedic implants. *Mater. Des.* **13**, 62–68 (2017)
13. Jiang, C.P., Wibisono, A.T., Pasang, T.: Selective laser melting of stainless 316L with face-centred-cubic based lattice structures to produce rib implants. *Materials* **14**, 5962 (2021)
14. Kladovasilakis, N., Tsongas, K., Kostavelis, I., Tzouvaras, D., Tzetzis, D.: Effective mechanical properties of additive manufactured strut-lattice structures: experimental and finite element study. *Adv. Eng. Mater.* **24**, 2100879 (2022)
15. Nazir, A., Arshad, A.B., Hsu, C.P., Jeng, J.Y.: Effect of fillets on mechanical properties of lattice structures fabricated using multi-jet fusion technology. *Materials* **14**(9), 2194 (2021)
16. Tang, C., Liu, J., Yang, Y., Liu, Y., Jiang, S., Hao, W.: Effect of process parameters on mechanical properties of 3D printed PLA lattice structures. *Composites Part C: Open Access* **3**, 100076 (2020)
17. Asadi-Eydivand, M., Solati-Hashjin, M., Farzad, A., Osman, N.A.A.: Effect of technical parameters on porous structure and strength of 3D printed calcium sulfate prototypes. *Robotics Computer-Integrated Manufacturing* **37**, 57–67 (2016)
18. Maskery, I., Aremu, A.U., Parry, L., Wildman, R.D., Tuck, C.J., Ashcroft, I.A.: Effective design and simulation of surface-based lattice structures featuring volume fraction and cell type grading. *Mater. Des.* **155**, 220–232 (2018)
19. Li, P.: Constitutive and failure behaviour in selective laser melted stainless steel for microlattice structures. *Material Science Eng.: A* **622**, 114–120 (2015)
20. Bai, L., Yi, C., Chen, X., Sun, Y., Zhang, J.: Effective design of the graded strut of bcc lattice structure for improving mechanical properties. *Materials* **12**, 2192 (2019)
21. Alberdi, R., et al.: Multi-morphology lattices lead to improved plastic energy absorption. *Mater. Des.* **194**, 108883 (2020)

**Open Access** This chapter is licensed under the terms of the Creative Commons Attribution 4.0 International License (<http://creativecommons.org/licenses/by/4.0/>), which permits use, sharing, adaptation, distribution and reproduction in any medium or format, as long as you give appropriate credit to the original author(s) and the source, provide a link to the Creative Commons license and indicate if changes were made.

The images or other third party material in this chapter are included in the chapter's Creative Commons license, unless indicated otherwise in a credit line to the material. If material is not included in the chapter's Creative Commons license and your intended use is not permitted by statutory regulation or exceeds the permitted use, you will need to obtain permission directly from the copyright holder.

